JOURNAL OF MATERIALS SCIENCE 30 (1995) 849–854

Toughening $MoSi_2$ with niobium metal – effects of morphology of ductile reinforcements

L. SHAW*
Systran Corporation, Dayton, OH 45432, USA
R. ABBASCHIAN
Department of Materials Science and Engineering, University of Florida, Gainesville, FL 32611, USA

Morphology effect of ductile reinforcements was evaluated using a four-point bend test on chevron-notched $MoSi_2$ composites reinforced with 20 vol. % niobium. The niobium used had three different morphologies, i.e., fibre, foil and particle. The thickness of the foils was 250 μm, while the fibres and particles had diameters of 250 and 200 μm, respectively. Toughness of $MoSi_2$ composites was increased from 3.3 MPa $m^{\frac{1}{2}}$ for the matrix to 15 MPa $m^{\frac{1}{2}}$ with the incorporation of the Nb fibres or foils. The particulate composites also exhibited an increase in toughness ($\sim$ 7 MPa $m^{\frac{1}{2}}$). The toughening achieved was mainly attributed to ductile phase bridging in all the composites tested. The relatively small toughness improvement in the particulate composites was ascribed to the embrittlement of the Nb particles. The results indicate that toughening by crack bridging depends mainly on the intrinsic properties of the ductile bridging ligaments rather than on their morphology, and that the embrittlement of the bridging ligament is detrimental to the toughening of the composites.

1. Introduction

It has been established that substantial toughening of brittle matrices can be achieved by incorporating ductile reinforcements. Examples of such systems are glass/Al [1, 2], glass/Ni [2], glass/Pb [3], glass/W [4], glass/Fe–Ni–Co alloy [5, 6], FeO/Fe [7], ZrO_2/Zr [8], MgO/Co, Fe or Ni [9], Al_2O_3/Mo [10], WC/Co [11], TiAl/Nb [12–14], TiAl/TiNb [13, 14], $MoSi_2$/Nb [15–22], Nb_5Si_3/Nb [23] and $NbAl_3$/Nb [24]. Although various degrees of toughening were observed in all the composites mentioned above, the most effective toughening was achieved in three composites: (1) WC reinforced with Co network (K_{IC} $\sim$ 20 MPa $m^{\frac{1}{2}}$ was obtained) [11]; (2) A K_{IC} of about 20 MPa $m^{\frac{1}{2}}$ was reached in TiAl with the addition of pancake-shaped Nb [12]; (3) Toughness of $MoSi_2$ was increased from 3.3 to about 15 MPa $m^{\frac{1}{2}}$ with the incorporation of Nb fibres or foils [17–19]. The results suggest that toughness of the ductile-phase-reinforced composites depends strongly on the microstructural design of the composites, i.e., the proper control and/or selection of various material parameters which include (1) the nature of the matrix/reinforcement interface, (2) size of the ductile phase, (3) intrinsic mechanical properties of the ductile phase and matrix, and (4) the morphology of the ductile phase.

Much effort has been made to systematically explore the effects of the matrix/reinforcement interfaces [2, 3, 14, 17–19, 25], size of ductile phases [3, 20, 22, 26], intrinsic properties of reinforcements [3, 14, 22, 27–29], and the proper combination of matrix and reinforcements [27, 28]. In contrast, systematic study on the effect of morphology is very scarce, although ductile phases with different geometries have been used to toughen various brittle materials by several investigators. So far, five kinds of morphologies of ductile phases have been used which are particles [1, 2, 5, 6, 9, 30], continuous boundary networks [7, 8, 11, 31], fibres [9, 15, 17, 21, 25], foils [17–22] and pancakes [12]. Toughening was observed in all the composites reinforced with continuous boundary networks, fibres, foils and pancakes, although it varied from system to system. The toughening in these composites is due to the special geometrical shapes of the ductile reinforcements which guarantee the crack/ductile phase interaction. However, for the particulate composites, some systems showed an increase in toughness [1, 2, 5, 6], while some did not [1, 2, 9]. The latter was when the matrix cracks were not attracted to ductile particles. These results clearly indicate that toughening is related to the morphology of ductile phases. Therefore, the present study is intended to systematically investigate the morphology effect of ductile phases on toughening using $MoSi_2$/Nb composites.

2. Experimental procedure

2.1. Fabrication of composites

Ductile phase, niobium (Nb), in the form of fibre, foil and particle was provided by Johnson Mathey Inc. Nb fibres and foils had a metallic impurity of 0.2 wt%, while the particles contained about 0.1–1 wt% Ta. The shape of the particles is irregular with sharp corners, as shown in Fig. 1. The thickness of the foils

*Previously known as L. Xiao.

0022–2461

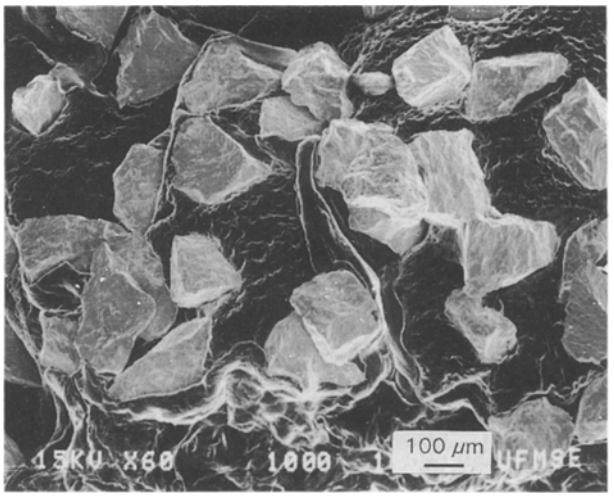

Figure 1 Secondary electron image of the as-received Nb particles.

was 250 μm, while the fibres and particles had a diameter of 250 and 200 μm, respectively. $MoSi_2$ powder with a median diameter of 1.12 μm was also supplied by Johnson Mathey Inc. The composition reported by the vendor was Mo > 61.0%, Si 36.6%, C 0.06%, N 0.03%, O 1.22% and metallic impurities < 0.5% (wt%).

For the Nb fibre-reinforced composites, the fibres were pre-aligned in a plane and set with acrylic resins. The fibre sheets were then stacked together with $MoSi_2$ powder in an appropriate thickness ratio. For the Nb foil-reinforced composites, the foils were simply alternatively stacked with $MoSi_2$ powder in the correct ratio, whereas for the particulate composites, Nb particles were ball milled with $MoSi_2$ powder for 24 hours before consolidation. All the composites fabricated contained 20 vol.% Nb and were consolidated via hot pressing at 1400 °C for 60 min under a pressure of 40 MPa.

2.2. Mechanical testing

Toughness of the composites was measured using four-point bend tests on chevron-notched specimens. Bend tests with an inner and outer span of 10 and 20 mm were carried out in a hydro-servo controlled MTS using a cross-head speed of 4×10^{-4} mm sec^{-1}. For comparison, toughness of monolithic $MoSi_2$ was also measured. To prepare the chevron notched specimens, the hot pressed discs were cut into rectangular bars with dimensions of $3.81 \times 5.08 \times 25.4$ mm. A notch on each sample was cut using a diamond wafering blade with a thickness of 0.15 mm. For the fibre-reinforced composites, the notch was cut perpendicular to the longitudinal direction of the fibres, while for the foil-reinforced composites, the notch was prependicular to the laminar plane.

The peak load of the bend test was used to calculate the toughness of the composites with the aid of the following equation [32]

$$K_{max} = \frac{P_{max}}{BW^{\frac{1}{2}}} Y^*_{min} \quad (1)$$

where P_{max} is the maximum test load, B and W are the width and height of the bending bar, respectively, and Y^*_{min} is the minimum value of the dimensionless stress intensity factor coefficient as a function of relative crack length for the particular specimen used. Because of the rising crack-growth resistance for ductile-phase-toughened composites, the maximum load and the minimum value of the dimensionless stress intensity factor coefficient do not occur coincidentally at the same crack length, and therefore P_{max} does not exactly correspond to the stress-intensity factor at failure, but is a good approximation to it [33–36]. The fact that P_{max} and Y^*_{min} do not occur coincidentally at the same crack length also induce a specimen size effect [33, 36]. Thus, the dimensions of the specimens in the present study were kept constant, and the value calculated using Equation 1 is called "damage tolerance" and designated as K_{max} in the paper, rather than K_{IC}.

3. Results and discussion

3.1. Mechanical behaviours of composites

Representative load-displacement curves of chevron-notched specimens for monolithic $MoSi_2$ and composites are shown in Fig. 2. The origin for each curve in this figure has been shifted for the convenience of observation. Note that the catastrophic failure of $MoSi_2$ has changed to graceful failure with the addition of niobium fibres and foils. Furthermore, the area under the load-displacement curve as well as the peak load have increased for all the composites, indicating an improvement in toughness. The damage tolerance, K_{max}, calculated from the peak load of the load-displacement curve using Equation 1 is summarized in Table I. It is clear from the table that composites reinforced with the fibres or foils have a much higher toughness than those reinforced with the particles. Furthermore, it is noted that the ductile fibres and foils have similar toughening capabilities.

3.2. Microstructures and fractographic characteristics of composites

The microstructures of the composites reinforced with 20 vol.% Nb fibres and particles are shown in Fig. 3.

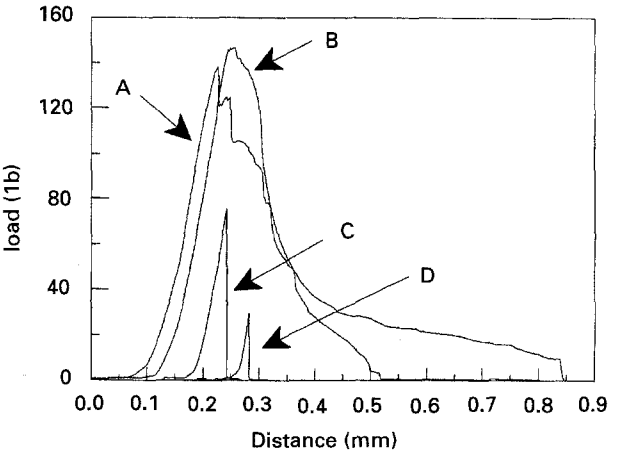

Figure 2 Typical load-displacement curves of chevron-notched monolithic $MoSi_2$ and composites containing 20 vol.% Nb. A, foil-reinforced; B, fibre-reinforced; C, particle-reinforced; D, monolithic $MoSi_2$.

TABLE I. Properties of monolithic $MoSi_2$ and composites with 20 vol.% Nb

	$MoSi_2$	Fibre-reinforced composites	Foil-reinforced composites	Particle-reinforced composites
K_{max} (MPa $m^{\frac{1}{2}}$	3.3 ± 0.3	15.2 ± 2.2	15.2 ± 1.3	7.5 ± 0.1
H_v of Nb ($kg\,mm^{-2}$)		163	145	264

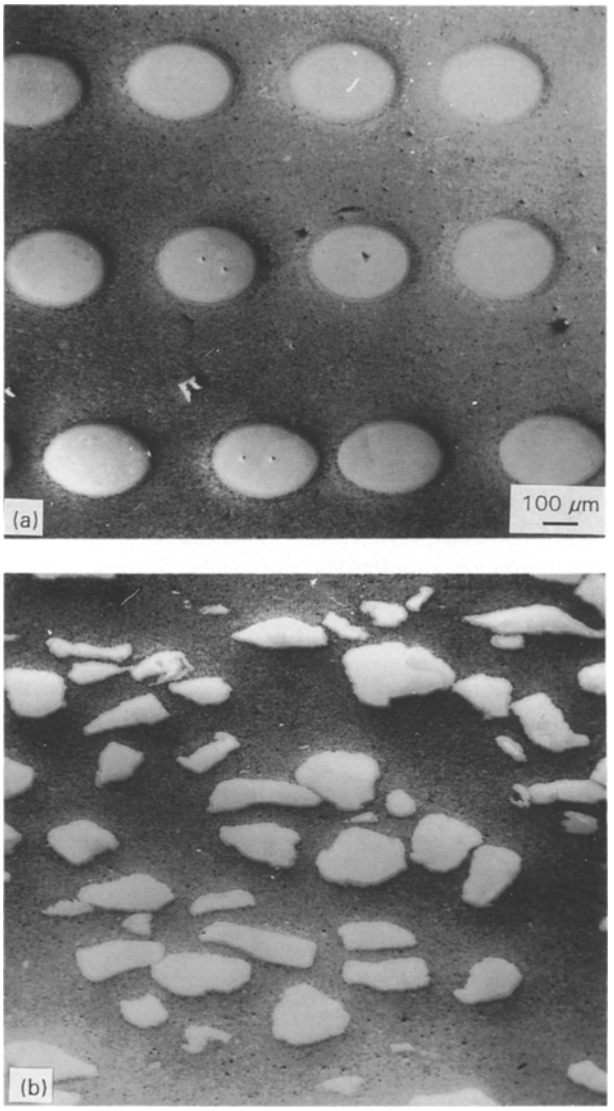

Figure 3 Microstructures of $MoSi_2$ composites reinforced with 20 vol.% of (a) Nb fibres and (b) particles.

The cross-sections shown are perpendicular to the hot press plane and the crack propagation is from bottom to top. Note that fairly uniform distribution of Nb reinforcements was achieved by the present processing routes, and that the niobium was deformed during the hot pressing, as is evident by the elliptical shape for the niobium filament and the irregularly elongated shape for the particle. It could be conceived that the deformed Nb particles actually became flattened spheres or even pancake-shaped in three dimensions. Because the crack propagation was perpendicular to the plane of the pancake or the flattened spheres (from bottom to top in Fig. 3), the deflection angle would be increased if crack deflection occurred, making the deflection in the present composites more energy consuming than in the composites with undeformed particles.

Overall views of representative fracture surfaces for the composites containing Nb reinforcements with different morphologies are provided in Fig. 4. Higher-magnification fractographs of the niobium in the composites are presented in Fig. 5 where the crack propagation is from bottom to top. There are several prominent features in these figures. First, the Nb fibres and foils exhibited both dimple and cleavage rupture, whereas the Nb particles almost exclusively showed cleavage rupture. Second, debonding at the matrix/reinforcement interface was observed in all the composites, although only a small portion of the interfaces did exhibit debonding in the particulate composites. Third, the particulate composites showed little evidence of particle pull-out. Finally, no reinforcement pull-out was observed in the fibre- and foil-reinforced composites.

Different fracture modes are believed to be due to the different intrinsic properties of the niobium rather than the difference in the niobium morphology. In a related study [18], it was shown that when Vickers hardness (H_v) of Nb was above 200 $kg\,mm^{-2}$, the Nb always fractured in cleavage mode. For the present case, the Nb particles had H_v of 264 $kg\,mm^{-2}$ after hot pressing, while the microhardness of the Nb fibres and foils was lower than 200 $kg\,mm^{-2}$ (Table I). The embrittlement of the Nb particles is likely related to the presence of small amounts of tantalum element in the as-received Nb particles. As such, the Nb particles fractured in cleavage mode, while the fibres and foils failed by dimple as well as cleavage rupture. In addition, because of the embrittlement, the bridging capability of the Nb particles decreased, and therefore crack became easier to cut through the particles, leading to negligible debonding at the interfaces. Furthermore, combination of the embrittlement and the irregular shape of the Nb particles with sharp corners gave rise to a situation that the particle pull-out was a higher energy-consuming process than the brittle fracture of the ductile phase. Therefore, there was almost no particle pull-out in the present case.

3.3. Ductile phase toughening

It has been established that the toughening of the foil-reinforced composites is due to the ductile phase bridging. For example, microstructure examination of the $MoSi_2$ composites reinforced with Nb foils unloaded at various levels of loading during the bend tests clearly showed the bridging of the ductile ligament [17]. Furthermore, in a recent study [26], the

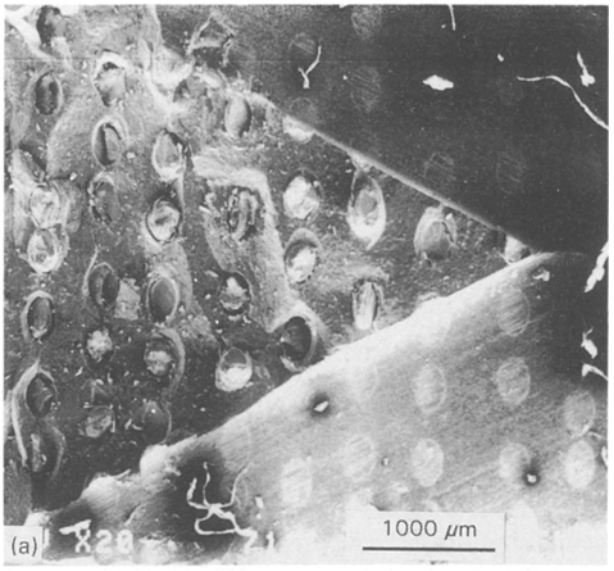

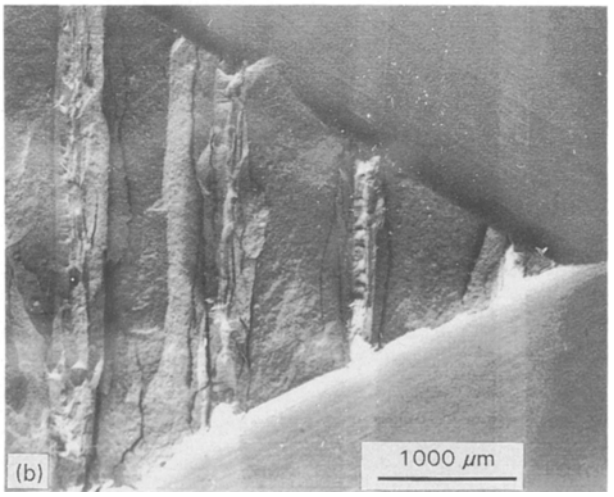

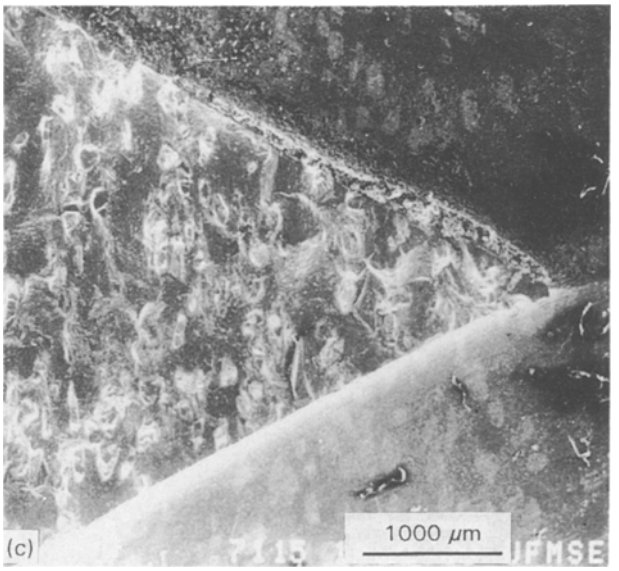

Figure 4 Fracture surfaces of the chevron-notched $MoSi_2$ composites containing 20 vol.% of (a) Nb fibres, (b) foils, and (c) particles.

damage tolerance of the foil-reinforced composites was related to the bridging contribution of the ductile reinforcement. The analysis indicated that the damage tolerance of the composites could be mainly accounted for by the bridging capability of the ductile laminae.

It is believed that ductile phase bridging is also the major mechanism responsible for the toughening of the present unidirectionally continuous fibre-reinforced composites, although debonding and crack deflection at the interfaces also contribute (Figs 4a and 5a). Thus, a comparison between the damage tolerances of the fibre- and foil-reinforced composites (Table I) leads to an important conclusion that is toughening depends mainly on the intrinsic properties of the bridging ligaments rather than on their morphologies, provided that crack bridging is the major toughening mechanism. The similar toughness of the fibre- and foil-reinforced composites implies that the bridging contributions of the fibres and foils are very similar. Usually, rods and bars have higher ultimate strength and larger elongation than plates at simple tensile tests, and this has been attributed to more restraint in the width direction in plates than in rods and bars [37, 38]. When ductile foils and fibres are embedded in a matrix, the difference in restraint between the two is expected to become smaller because both the reinforcements experience high constraint from the matrix. As such, a similar bridging contribution from the two morphologies results.

The similar toughness of the fibre- and foil-reinforced composites has a bearing on the design of ductile-phase-toughened composites. A recent study [26] has demonstrated that due to different morphologies, of ductile reinforcements, foil-reinforced composites provide two-dimensional toughening, while unidirectionally continuous fibre-reinforced composites only give one-dimensional toughening. Combination of these two studies suggests that ductile foils can, in fact, provide better toughening characteristics than ductile fibres without sacrificing the toughness of the composites.

For the present particulate composites, a toughness increase of about 1.3 times over the monolithic $MoSi_2$ was observed (Table I). This increment falls into the range of toughening by crack deflection mechanism. Faber and Evans [39, 40] have shown that about one-fold increase in toughness can be achieved by crack deflection due to the addition of spherical particles, and that as high as three-fold increases can be reached by crack deflection with rod-shaped particles of high aspect ratio. Although the toughness increment in the current particulate composites falls into the range of toughening predicted by crack deflection mechanism [39, 40], examination of fracture surfaces of the composites did not show the circumvention of the Nb particles by cracks, a phenomenon of crack deflection by particles. Instead, cracks almost exclusively cut through the Nb particles (Fig. 5c), an indication of crack bridging and/or crack blunting. The crack bridging was further supported by the examination of the propagation profile of the indentation cracks on the polished surface. As shown in Fig. 6, a crack induced by a Vickers indentation ran into Nb particle directly, were blunted by the particle and initiated another crack at the other side of the particle (as indicated by the arrow in the figure), rather than being deflected or causing the debonding at the

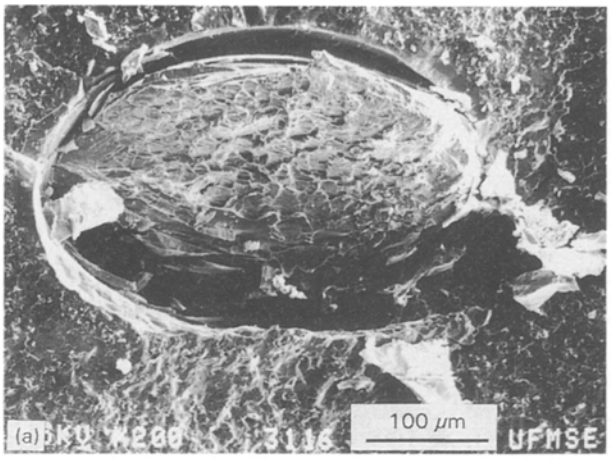

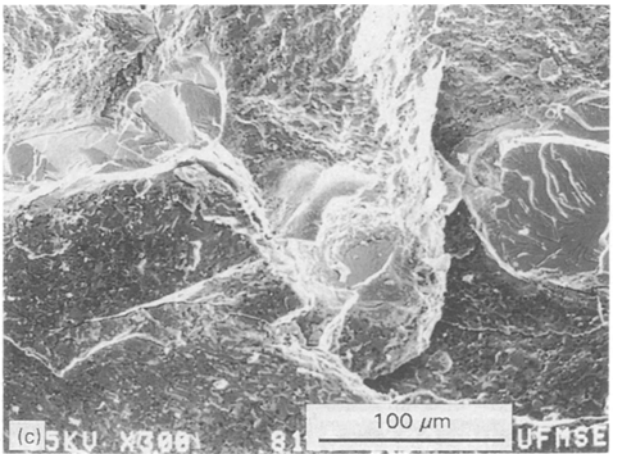

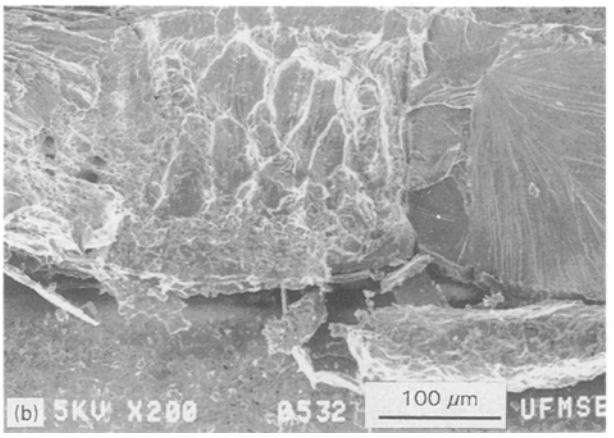

Figure 5 Fracture surfaces of (a) Nb fibres, (b) foils and (c) particles in the chevron-notched $MoSi_2$ composites with crack propagation from bottom to top.

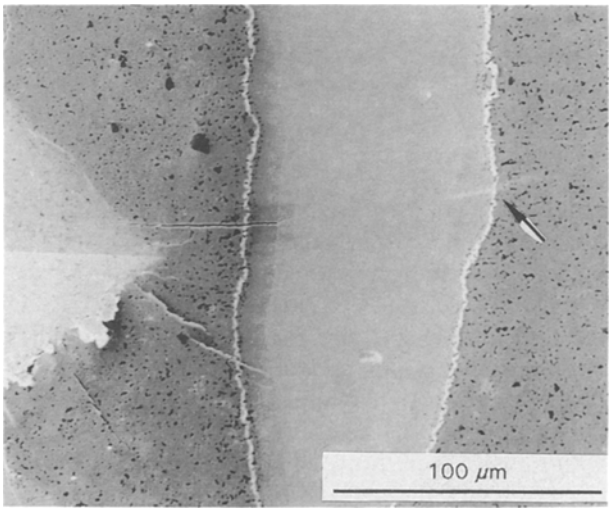

Figure 6 Interaction between a Nb particle and cracks introduced by a Vickers indentor on the polished surface of a particulate composite.

interface. The relatively small toughness increase in the particulate composites may be explained by the embrittlement of the Nb particles discussed in the previous section. It had been shown [18] that the embrittlement of bridging ligaments was accompanied by a decrease in the toughness of the composites. For example, toughness of composites containing 20 vol.% Nb foils decreased from 12.8 to 8.6 MPa $m^{\frac{1}{2}}$ when H_v of the Nb reinforcement increased from 131 to 236 kg $mm^{\frac{1}{2}}$ owing to the inappropriate processing conditions [18]. It is thus concluded that toughening of the particulate composites is due to the crack bridging and the relatively small increase in toughness is ascribed to the embrittlement of the ductile particles.

Finally, it should be pointed out that even without the embrittlement of the reinforcement, the particulate composites may still not be able to reach the toughness exhibited by the fibre- or foil-reinforced composites. When there is no embrittlement, several other mechanisms may set in before the full operation of the crack bridging mechanism. For example, crack deflection may happen which could only lead to as high as four-fold toughness of the matrix [39, 40]. For the present matrix (K_{max} = 3.3 MPa $m^{\frac{1}{2}}$); this maximum toughness available due to the crack deflection is about 12 MPa $m^{\frac{1}{2}}$, a value still lower than those displayed by the present foil- and fibre-reinforced composites. Another mechanism that may occur is interfacial debonding which would allow more ductile phase to deform and adsorb more energy before the failure of the composites. A recent study [22] has shown that the interfacial debonding length is proportional to the representative cross-sectional diameter of the reinforcement, and typically, the debonding length is at least two times the representative diameter when the crack bridging mechanism operates fully. Thus, the bridging particles should have a high aspect ratio and be longer than twice the representative diameter. As such, the two ends of the particles can still be embedded in the matrix after the debonding and the clamping forces of the bridging particles can, therefore, be transferred onto the crack faces. The load transfer length, i.e., the embedded length of the particle end required for the full operation of the crack bridging, depends on the shear strength of the interface and the toughness of the matrix, and therefore varies from one composite system to another. Usually, the shear strengths of ductile metals are about half of their tensile strengths. Thus, if the tensile strength of Nb is taken as 285 MPa [22], then its shear strength is about 140 MPa. If it is further assumed that the shear strength of Nb is the controlling strength at the interface, and the maximum bridging stress is taken as 350 MPa [22], then the full load transfer length should be 125 μm calculated by equating the ligament

breaking load with the interfacial shear force for 200 μm diameter particles. Thus, the aspect ratio of the bridging particles should be at least 3.25 for the full load transfer. For the present particulate composites, even though the particles have been deformed and elongated along the hot press plane, their aspect ratio is generally still lower than 3.25, as shown in Fig. 3. Thus, it is quite clear that even without the embrittlement, the particulate composites still cannot reach the toughness of fibre- or foil-reinforced composites. If a high toughness is expected, particles with a high aspect ratio and some processing procedures for the alignment of the particles should be utilized.

4. Implications and conclusions

Morphology effect of ductile reinforcements has been evaluated using a four-point bend test on chevron-notched $MoSi_2$ composites reinforced with 20 vol.% niobium. Toughness of $MoSi_2$ composites has been increased from 3.3 MPa $m^{\frac{1}{2}}$ for the matrix to 15 MPa $m^{\frac{1}{2}}$ with the incorporation of 20 vol.%. Nb fibres or foils. The addition of Nb particles also increases the toughness to $\sim$ 7 MPa $m^{\frac{1}{2}}$. The toughening has been ascribed to the ductile phase bridging in all the composites tested. The results suggest that (1) toughening by crack bridging depends mainly on the intrinsic properties of the ductile ligaments rather than on their morphology; (2) ductile foils could provide two-dimensional toughening without sacrificing the toughness of the composites, while ductile fibres only supply one-dimensional toughening; (3) the embrittlement of ductile reinforcements is detrimental to the toughening of the composites; and (4) particles with a high aspect ratio should be used if particulate composites are designed to approach the toughness of fibre- and foil-reinforced composites.

Acknowledgements

The authors are grateful to the support of the Advanced Research Projects Agency (ARPA) and Office of Naval Research through grant N00014-91-J-4075.

References

1. A. K. KHAUND and P. S. NICHOLSON, *J. Mater. Sci.* **15** (1980) 177.
2. V. V. KRSTIC, P. S. NICHOLSON and R. G. HOAGLAND, *J. Amer. Ceram. Soc.* **64** (1981) 499.
3. M. F. ASHBY, F. J. BLUNT and M. BANNISTER, *Acta Metall.* **37** (1989) 1847.
4. Y. NIVAS and R. M. FULRATH, *J. Amer. Ceram. Soc.* **53** (1970) 188.
5. T. L. JESSEN, J. J. MECHOLSKY and R. H. MOORE, *Amer. Ceram. Soc. Bull.* **65** (1986) 377.
6. J. J. MECHOLSKY, T. L. JESSEN and R. H. MOORE, *Ceram. Eng. Sci. Proc.* **6** (1985) 657.
7. M. I. MENDELSON and M. E. FINE, *J. Amer. Ceram. Soc.* **57** (1974) 154.
8. A. V. VIRKAR and D. L. JOHNSON, *J. Amer. Ceram. Soc.* **60** (1977) 514.
9. P. HING and G. W. GROVES, *J. Mater. Sci.* **7** (1972) 427.
10. D. T. RANKIN, J. J. STIGLICH, D. R. PETRAK and E. RUH, *J. Amer. Ceram. Soc.* **54** (1971) 277.
11. J. L. CHERMANT and F. OSTERSTOCK, *J. Mater. Sci.* **11** (1976) 1939.
12. C. K. ELLIOTT, G. R. ODETTE, G. E. LUCAS and J. W. SHECKHERD, in "High Temperature, High Performance Composites", Proceedings of MRS Symposium, edited by F. D. Lemkey, S. G. Fishman, A. G. Evans and J. R. Strife, Materials Research Society, 1988) pp. 95–102.
13. H. C. CAO, B. J. DALGLEISH, H. DEVE, C. ELLIOTT, A. G. EVANS, R. MEHRABIAN and G. R. ODETTE, *Acta Metall.* **37** (1989) 2969.
14. H. E. DEVE, A. G. EVANS, G. R. ODETTE, R. MEHRABIAN, M. L. EMILIANI and R. J. HECHT, *Acta Metall. Mater.* **38** (1990) 149.
15. E. FITZER, in "Whisker- and Fiber-Toughened Ceramics," edited by R. A. Bradley D. E. Clark, D. C. Larsen and J. O. Stiegler, (ASM International, 1988) pp. 165–92.
16. T. C. LU, A. G. EVANS, R. J. HECHT and R. MEHRABIAN, *Acta Metall. Mater.* **39** (1991) 1853.
17. L. XIAO, Y. S. KIM, R. ABBASCHIAN and R. J. HECHT, *Mater. Sci. Eng.* **A144** (1991) 277.
18. L. XIAO and R. ABBASCHIAN, *Metall. Trans.* **23A** (1992) 2863.
19. L. XIAO and R. ABBAASCHIAN, *Mater. Sci. Eng.* **A155** (1992) 135.
20. L. XIAO and R. ABBASCHIAN, in "Advanced Metal Matrix Composites for Elevated Temperatures", edited by M. N. Goungor, E. J. Lavernia and S. G. Fishman, (ASM International, 1991) pp. 21–31.
21. L. XIAO, Y. S. KIM and R. ABBASCHIAN, in "Intermetallic Matrix Composites", Proceedings of MRS Symposium, edited by D. L. Anton, P. L. Martin, D. B. Miracle and R. McMeeking, (Materials Research Society, 1990) pp. 399–404.
22. L. XIAO and R. ABBASCHIAN, *Metall. Trans.* **24A** (1993) 403.
23. J. J. LEWANDOWKI, D. DIMIDUK, W. KERR and M. G. MENDIRATTA, in "High Temperature, High Performance Composites", Proceedings of MRS Symposium, edited by F. D. Lemkey, S. G. Fishman, A. G. Evans and J. R. Strife, (Materials Research Sociey, 1988) pp. 103–9.
24. L. LU, A. B. GOKHALE and R. ABBASCHIAN, *Mater. Sci. Eng.* **A144** (1991) 11.
25. H. E. DEVE and M. J. MALONEY, *Acta Metall. Mater.* **39** (1991) 2275.
26. L. SHAW and R. ABBASCHIAN, *Acta Metall. Mater.* **42** (1994) 213.
27. L. SHAW and R. ABBASCHIAN, *Acta Metall. Mater* in press.
28. K. S. RAVICHANDRAN, *Acta Metall. Mater.* **40** (1992) 1009.
29. B. N. COX, *Acta Metall. Mater* **39** (1991) 1189.
30. D. J. GREEN, P. S. NICHOLSON, and J. D. EMBURY, *J. Mater. Sci.* **14** (1979) 1413.
31. L. S. SIGL and H. F. FISCHMEISTER, *Acta Metall.* **36** (1988) 887.
32. D. G. MUNX, J. L. SHANNON, Jr., and R. T. BUSEY, *Int. J. Fracture* **16** (1980) 137.
33. J. C. NEWMAN, Jr., in "Chevron-Notched Specimens: Testing and Stress Analysis", ASTM STP 855, edited by J. H. Underwood, S. W. Freiman and F. I. Baratta (American Society for Testing and Materials, 1984) pp. 5–31.
34. L. M. BARKER and F. I. BARATTA, *J. Testing Evaluation* **8** (1980) 97.
35. D. MUNZ, *Eng. Fracture Mech.* **15** (1981) 231.
36. J. L. SHANNON, Jr. and D. G. MUNZ, in "Chevron-Notched Specimens: Testing and Stress Analysis". ASTM STP 855, edited by J. H. Underwood, S. W. Freiman and F. I. Baratta (American Society for Testing and Materials, 1984) pp. 270–80.
37. J. MIKLOWITZ, *J. Appl. Mech.* **70** (1948) 274.
38. J. MIKLOWITZ, *J. Appl. Mech.* **70** (1950) 274.
39. K. T. FABER and A. G. EVANS, *Acta Metall* **31** (1983) 565.
40. K. T. FABER and A. G. EVANS, *Acta Metall.* **31** (1983) 577.

Received 13 April
and accepted 6 July 1994